THE JOURNAL OF BIOLOGICAL CHEMISTRY VOL. 288, NO. 9, pp. 6363–6370, March 1, 2013

Structural Basis for a Bispecific $NADP^+$ and CoA Binding Site in an Archaeal Malonyl-Coenzyme A Reductase*

Received for publication, September 21, 2012, and in revised form, January 7, 2013 Published, JBC Papers in Press, January 16, 2013, DOI 10.1074/jbc.M112.421263

Ulrike Demmer[‡1], Eberhard Warkentin[‡1], Ankita Srivastava[‡], Daniel Kockelkorn[§], Markus Pötter[¶], Achim Marx[¶], Georg Fuchs[§], and Ulrich Ermler[‡2]

From the [‡]Max-Planck-Institut für Biophysik, D-60438 Frankfurt am Main, Germany, [§]Mikrobiologie Institut für Biologie II, Universität Freiburg, D-79104 Freiburg, Germany, and [¶]Evonik Industries AG, D-45128 Essen, Germany

Background: Malonyl-CoA reductase of the CO_2 assimilating 3-hydroxypropionate/4-hydroxybutyrate cycle reduces malonyl-CoA to malonic semialdehyde.
Results: Malonyl-CoA reductase complexed with CoA and $NADP^+$ was structurally characterized.
Conclusion: The protein acts as rigid template to press CoA and $NADP^+$ into similar S-shaped, superimposable forms.
Significance: The data indicate how to construct a bispecific cofactor binding site and to engineer a malonyl- into methylmalonyl-CoA reductase for polyester building block production.

Autotrophic members of the Sulfolobales (crenarchaeota) use the 3-hydroxypropionate/4-hydroxybutyrate cycle to assimilate CO_2 into cell material. The product of the initial acetyl-CoA carboxylation with CO_2, malonyl-CoA, is further reduced to malonic semialdehyde by an NADPH-dependent malonyl-CoA reductase (MCR); the enzyme also catalyzes the reduction of succinyl-CoA to succinic semialdehyde onwards in the cycle. Here, we present the crystal structure of *Sulfolobus tokodaii* malonyl-CoA reductase in the substrate-free state and in complex with $NADP^+$ and CoA. Structural analysis revealed an unexpected reaction cycle in which $NADP^+$ and CoA successively occupy identical binding sites. Both coenzymes are pressed into an S-shaped, nearly superimposable structure imposed by a fixed and preformed binding site. The template-governed cofactor shaping implicates the same binding site for the 3′- and 2′-ribose phosphate group of CoA and $NADP^+$, respectively, but a different one for the common ADP part: the β-phosphate of CoA aligns with the α-phosphate of $NADP^+$. Evolution from an $NADP^+$ to a bispecific $NADP^+$ and CoA binding site involves many amino acid exchanges within a complex process by which constraints of the CoA structure also influence $NADP^+$ binding. Based on the paralogous aspartate-β-semialdehyde dehydrogenase structurally characterized with a covalent Cys-aspartyl adduct, a malonyl/succinyl group can be reliably modeled into MCR and discussed regarding its binding mode, the malonyl/succinyl specificity, and the catalyzed reaction. The modified polypeptide surrounding around the absent ammonium group in malonate/succinate compared with aspartate provides the structural basis for engineering a methylmalonyl-CoA reductase applied for biotechnical polyester building block synthesis.

Autotrophic members of the archaeal order Sulfolobales (Crenarchaeota) use acetyl-CoA/propionyl-CoA carboxylase as the primary CO_2 fixing enzyme in the 3-hydroxypropionate/4-hydroxybutyrate cycle (1–6). This cycle starts with acetyl-CoA carboxylation to malonyl-CoA, which is further reduced by malonyl-CoA reductase (MCR)[3] catalyzing the following: malonyl-CoA + NADPH + H^+ → malonic semialdehyde + $NADP^+$ + CoA (see Fig. 1*A*) (7). The enzyme is unrelated to the bifunctional malonyl-CoA reductase in some bacteria that catalyzes, in addition, the reduction of malonic semialdehyde to 3-hydroxypropionate (8, 9). Yet, the archaeal enzyme catalyzes also the reduction of succinyl-CoA onwards in the autotrophic cycle (10), which is required for regeneration of the starting molecule acetyl-CoA: succinyl-CoA + NADPH + H^+ → succinic semialdehyde + $NADP^+$ + CoA (see Fig. 1*A*).

Sequence comparison suggests that the archaeal malonyl-CoA reductase gene (*mcr*) has evolved from the duplication of a common ancestral aspartate-β-semialdehyde dehydrogenase (ASD) gene (*asd*) and has since diverged from the parent copy by mutation and selection to achieve its new function. Aspartate-semialdehyde dehydrogenase catalyzes as follows: aspartyl-4-phosphate + NADPH + H^+ → aspartic β-semialdehyde + $NADP^+$ + inorganic phosphate (Fig. 1*B*). The two paralogous MCR and ASD enzymes show ~40% amino acid sequence identity in the same organism, and their genes *mcr* and *asd* have different chromosomal locations. The *mcr* gene occurs only in autotrophic Sulfolobales underlining its role in the carbon fixation cycle and its neighbor genes are generally not conserved among different species. The *asd* gene clusters together with threonine synthase, aspartokinase, and ornithine carbamoyltransferase, among other genes, which is in line with its role in the biosynthesis of amino acids of the aspartate family.

MCR is a homotetramer. The monomer (M_r of 39 kDa) is topologically classified as member of the GADPH family. Activity is stimulated by thiols and inactivated by thiol-

* This work was supported by Deutsche Forschungsgemeinschaft (Fu 118/15-4) and Evonik Industries AG.
The atomic coordinates and structure factors (codes 4DPK, 4DPL, and 4DPM) have been deposited in the Protein Data Bank (http://wwpdb.org/).
[1] Both authors contributed equally to this work.
[2] To whom correspondence should be addressed: Max-Planck-Institut für Biophysik, Max-von-Laue-Straβe 3, D-60438 Frankfurt am Main, Germany. Tel.: 49-0-69-6303-1054; Fax: 49-0-69-6303-1002; E-mail: ulrich.ermler@biophys.mpg.de.

[3] The abbreviations used are: MCR, malonyl (succinyl)-CoA reductase; ASD, aspartate-β-semialdehyde dehydrogenase; GAPDH, glyceraldehyde-3-phosphate dehydrogenase; CoA, coenzyme A.

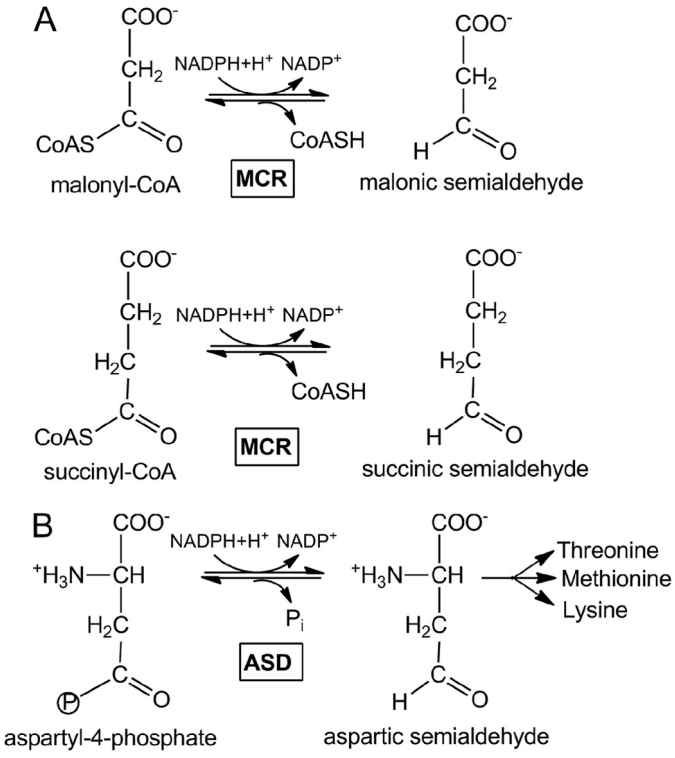

FIGURE 1. **Reactions catalyzed by MCR (*A*) and ASD (*B*).**

blocking agents suggesting an essential role of a cysteine residue in catalysis (7). In fact, one conserved cysteine and histidine are crucial for catalysis of this enzyme class. Interestingly, recombinant malonyl-CoA reductase binds small RNA of 60 to 180 nucleotides, which could be a hint for nonspecific cleaving of RNA (7). RNA cleavage has been shown for other metabolic enzymes, *e.g.* glyceraldehyde-3-phosphate dehydrogenase; however, the physiological role is not known (11, 12).

An x-ray structure was so far not reported for MCR but for homologous enzymes, with the most related being the well characterized aspartate-β-semialdehyde dehydrogenase (ASD) (13). However, MCR catalyzes a different reaction, which might implicate significant differences in the active site architecture and the enzymatic mechanism. In addition, MCR is also of biotechnological interest for the production of polyester building blocks. It may be used either for production of 3-hydroxypropionate (precursor of acrylate) from malonyl-CoA, or for production of 3-hydroxyisobutyrate (precursor of methacrylate) from methylmalonyl-CoA using an engineered enzyme.

For a more profound understanding of substrate binding and the catalyzed reaction and for a rational design of a productive methylmalonyl-CoA reductase detailed structural information is indispensable, which prompted us to initiate an x-ray crystallographic analysis of MCR. The determined structures of substrate-free MCR and of MCR in complex with $NADP^+$ (MCR_{NADP}) and CoA (MCR_{CoA}) reveal insights into the geometry and evolution of a bispecific cofactor binding site.

EXPERIMENTAL PROCEDURES

Heterologous production of the Sulfolobus tokodaii MCR in Escherichia coli—Materials used, strains and culture conditions, preparation of cell extract, enzyme assay, heterologous expression of the malonyl-CoA reductase (*mcr*) gene from *S. tokodaii*, production of the protein in *E. coli*, and purification of heterologously expressed malonyl-CoA reductase have been described (7, 10).

In brief, *S. tokodaii* (Deutsche Sammlung von Mikroorganismen und Zellkulturen 16993) (14) was grown aerobically and heterotrophically at 75 °C on a chemically defined medium (pH 3.0) with 1 g per liter of glucose (generation time, 6 h). Cells were stored in liquid nitrogen until use. *E. coli* strain Rosetta 2 (Merck) was grown at 37 °C in Luria-Bertani (LB) medium. Antibiotics were added to *E. coli* cultures to the following final concentration: ampicillin, 100 μg ml^{-1}; chloramphenicol, 34 μg ml^{-1}.

Harvested cells were resuspended in a 2-fold volume of 50 mM Tris/HCl, pH 7.8, containing 5 mM $MgCl_2$ and 0.1 mg ml^{-1} DNase I. The cell suspension was passed through a French pressure cell at 137 megapascal and ultracentrifuged (100,000 × *g*) at 4 °C for 1 h. The cell extract was used immediately or kept frozen at −70 °C. The malonyl-CoA-dependent oxidation of NADPH was followed spectrophotometrically at 365 nm ($\epsilon_{365\ nm}$ NADPH = 3,400 M^{-1} cm^{-1}). Similarly, the reductions of succinyl-CoA and of methylmalonyl-CoA were followed. Chromosomal DNA from *S. tokodaii* was isolated using standard techniques. Two synthetic oligonucleotides were designed to amplify the complete *mcr* gene using chromosomal DNA from *S. tokodaii* as a template (for genome, see Ref. 15), and the sequence of the insert was checked. The plasmid pTrc99A was digested with NcoI and BamHI, and the plasmid pTrc99A-Mcr was generated after ligation of the fragment with the *mcr* gene. A plasmid-derived *lac* promotor in front of *mcr* allows expression of the gene after induction of isopropyl thiogalactopyranoside. Competent *E. coli* Rosetta 2 cells were transformed with pTrc99A-Mcr, grown in a 200-liter fermenter at 37 °C in LB broth containing 100 μg of ampicillin ml^{-1}, and induced at an optical density of 0.6 (1-cm light path) with 0.5 mM isopropyl thiogalactopyranoside. After additional growth for 3 h, the cells were harvested and stored in liquid nitrogen until use.

Purification of the Recombinant Enzyme—The recombinant enzyme was purified from the supernatant of the cell extract after centrifugation at 100,000 × *g* (starting normally from 10 g (wet weight) of cells of *E. coli*) in three steps: 1) heat precipitation at 85 °C and concentration by ultrafiltration (Amicon YM30 membrane, Millipore); 2) gel filtration chromatography using a Superdex 200 HR 26/60 gel filtration column (Pharmacia; diameter, 2.6 cm; volume, 320 ml); and 3) Resource Phenyl chromatography using a Resource Phenyl column (1 ml of Resource PHE, Amersham Biosciences). According to SDS-PAGE, the enzyme was pure.

Crystallization and X-ray Structure Determination—MCR from *S. tokodaii* was concentrated to 15 mg/ml in 10 mM Hepes, pH 7.0, 5 mM $MgCl_2$ (only in some cases used) and 100 mM NaCl and crystallized at a temperature of 18 °C using the sitting drop method. Successful crystallization experiments were under-

TABLE 1
X-ray crystallographic statistics

Crystallization and data collection	$MCR_{substrate-free}$	MCR_{NADP}	MCR_{CoA}
Protein solution	10 mM HEPES, pH 7.0, 0.1 M NaCl	10 mM HEPES, pH 7.0, 0.1 M NaCl, 5 mM $NADP^+$	10 mM HEPES, pH 7.0, 0.1 M NaCl, 5 mM $NADP^+$, 5 mM succinyl-CoA
Conditions[a]	34% MPD, 0.1 M Hepes pH 7.5, 100 mM $CaCl_2$	33% PEG 426, 0.1 M NaOAc, pH 4.6, 0.15 M $(NH_4)_2SO_4$	11% PEG 6000, 10 mM $MgCl_2$
Space group	*C*2	$P2_12_12_1$	$C222_1$
Unit cell parameter (Å)	167.1, 81.9, 124.6 105.0°	94.7, 128.8, 140.5	111.6, 137.6, 363.0
Nr. mol/asymmetrical unit	1 tetramer	1 tetramer	1.5 tetramer
Detector	MARCCD 225 mm	PILATUS 6 M	MARCCD 225 mm
Wavelength (Å)	0.9764	1.0	0.9999
Resolution (Å) (highest shell)	50.0-2.05 (2.1-2.05)	50.0-1.9 (2.0-1.9)	50.0-2.4 (2.5-2.4)
R_{sym} (%)	5.8 (25.8)	5.5 (45.6)	6.4 (41.4)
$I/\sigma(I)$	15.0 (4.5)	15.5 (3.2)	20.5 (3.9)
Completeness (%)	95.8 (74.2)	99.5 (99.2)	92.5 (65.4)
Redundancy	4.1 (2.8)	3.8 (3.8)	7.0 (4.4)
Refinement			
Resolution (Å) (highest shell)	20.0-2.05 (2.10-2.05)	20.0-1.9 (1.95-1.9)	30.0-2.4 (2.46-2.4)
R_{cryst}/R_{free} (%) (highest shell)	18.5/23.1 (23.1/26.3)	16.3/19.4 (25.2/29.2)	20.2/24.5 (34.8/38.2)
No. of residues	4 × 360	4 × 354	6 × 355
No. of solvent molecules	500	891	557
r.m.s.d. bond lengths (Å)	0.017	0.021	0.019
r.m.s.d. bond angles	1.58°	1.82°	1.72°
Average B ($Å^2$) Protein/ligand/solvent	44.2/NA/39.0[b]	34.7/53.3/38.9	35.5/43.9/48.7[c]
PDB accession code	4DPK	4DPL	4DPM

[a] Crystals were originally found in the JBScreen Classic kit (Jena Bioscience) and optimized by own solutions.
[b] NA, not available; r.m.s.d., root mean square deviation.
[c] The values are only related to the polypeptide and CoA of chains A and B.

taken with MCR and MCR supplemented with $NADP^+$ or malonyl/succinyl-CoA. The detailed conditions are listed in Table 1. Data were collected at the SLS-PXII beamline (Villigen) and processed with XDS (16). The structure of $MCR_{substrate-free}$ from *S. tokodaii* was determined at 2.05 Å resolution by the molecular replacement method (17) using the ASD model of *Methanococcus jannaschii* (18). Model building and refinement were performed with COOT (19) and REFMAC (20), respectively. The obtained MCR model was subsequently applied to solve MCR_{NADP} and MCR_{CoA} structures. Refinement was performed using mostly "medium/loose" non-crystallographic symmetry restraints for the main and side chains of $MCR_{substrate-free}$, MCR_{NADP}, and MCR_{CoA}. Translation, libration, and screw-motion parameters were also refined using one monomer as group. The root mean square deviations between $MCR_{substrate-free}$ and MCR_{NADP}, $MCR_{substrate-free}$, and MCR_{CoA}, and MCR_{NADP} and MCR_{CoA} structures are 0.3 Å, 0.4 Å, and 0.3 Å, respectively, using C_α atoms for calculations. Crystallographic data are summarized in Table 1. Figs. 2–4 were generated with PyMOL (Schrodinger, LLC). Atomic coordinates and structure factors of $MCR_{substrate-free}$, MCR_{NADP}, and MCR_{CoA} have been deposited in the Protein Data Bank under codes 4DPK, 4DPL, and 4DPM.

RESULTS AND DISCUSSION

Overall Architecture of MCR—The structure of recombinantly produced MCR of *S. tokodaii* was characterized at 2.05 Å resolution in a substrate-free state (Table 1). The enzyme shows, as expected, a GAPDH-like fold (Fig. 2), the most related family members are ASD, *N*-acetyl-γ-glutamyl phosphate reductase, and GAPDH with root mean square deviations between 1.4 and 2.6 Å for the corresponding *M. jannaschii* (Protein Data Bank code 1YS4), *Salmonella typhimurium* (Protein Data Bank code 2G17), and *Bacillus thermophilus* (Protein Data Bank code 1GD1) enzymes. The structures of MCR and the most related ASD from *M. jannaschii* deviate only in a few loop segments in the order of maximally 3 Å except for the loop after helix 204:219 (deviation > 20 Å).

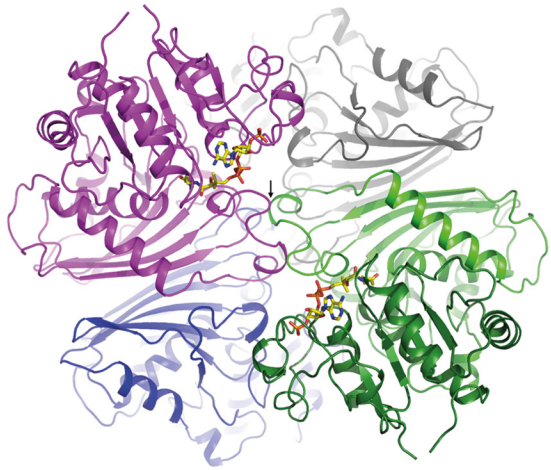

FIGURE 2. **Structure of MCR from *S. todokaii*.** The MCR homotetramer is arranged as a dimer of dimers (colored in *magenta/blue* and *gray/green*). Each monomer is built up of a dinucleotide binding (*dark green*) and a dimerization domain (*light green*). The active site cleft lies between them and is occupied in the MCR_{CoA} structure by CoA (drawn as a stick model). Two dimers form an extended interface that includes both cover loops (*black arrow*) being involved in substrate binding.

In agreement with previous solution data (7), MCR was found in the crystal structure as a homotetramer that is organized as a dimer of two dimers (Fig. 2). Each monomer is composed of a classical dinucleotide binding domain and a dimerization domain consisting of a mixed six-stranded β-sheet primarily flanked by three α-helices on one side and the dimerization domain of the counter subunit on the other side. The two central β-sheets of the dimerization domains face each other, thereby forming an extended monomer-monomer con-

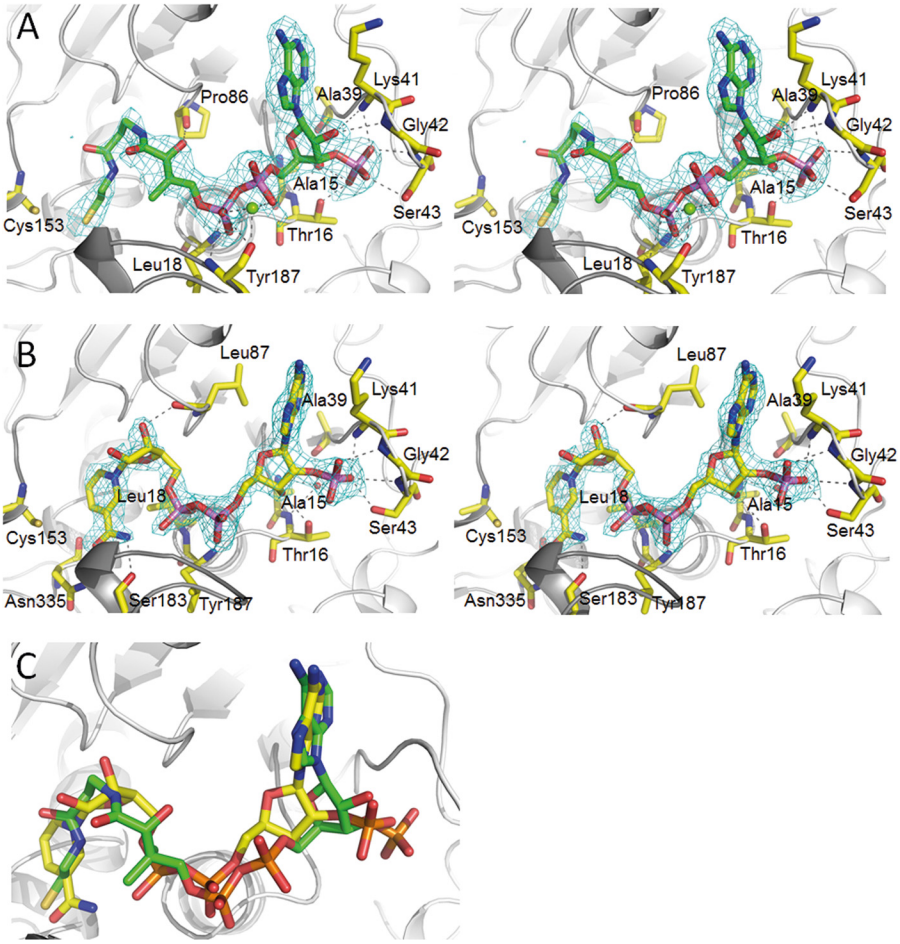

FIGURE 3. **Cofactor binding to MCR.** *A*, $NADP^+$ binding in stereo. $NADP^+$ binds in a characteristic S-shaped conformation and is sandwiched between the loops of the C-terminal end of the β-sheet (*light gray*) and the cover loop (*dark gray*). Only residues forming hydrogen bonds to the polypeptide are shown. $NADP^+$ is firmly anchored to the polypeptide at the 2′-ribose phosphate binding site. Proton donors comprise Lys^{41} NH, Gly^{42} NH, Ser^{43} NH, Ser^{43} $O_\gamma H$, and Thr^{16} $O_{\gamma 1}H$ as well as via a solvent molecule Ala^{39} O, Thr^{16} NH, and Ala^{15} NH. The $2F_{obs} - F_{calc}$ electron density (*cyan*) is drawn at a contour level of 1.3σ. *B*, CoA binding in stereo. CoA is arranged in an S-shaped, rather compressed conformation (distance between α-phosphate O2A and β-cysteamine N4P, 8.7 Å) and embedded into the same binding site as $NADP^+$. A metal ion seems to be positioned between the α- and β-phosphate and the Tyr^{187} carbonyl oxygens. The $2F_{obs} - F_{calc}$ electron density (*cyan*) is drawn at a contour level of 1.5σ. *C*, superposition of $NADP^+$ and CoA. The carbons of $NADP^+$ are colored in *yellow*, and CoA carbons are in *green*. The distances between the β-phosphate of CoA and the α-phosphate of $NADP^+$ and between their 3′- and 2′-ribose phosphates are ~1.4 Å.

tact area (Fig. 2). The two dimers of MCR forming the tetramer are stacked on each other at right angles and possess an interface at their centers (Fig. 2) that is conserved in GAPDH-like family members. However, tetramerization is not uniformly maintained (*i.e.* ASD is a dimer). No electron density was visible for RNA that strongly binds in substantial amounts to recombinant MCR (7) suggesting a flexible binding at the protein surface (if bound at all in the crystalline state).

The substrate binding site of MCR (and the entire GAPDH-like family) is accommodated in a mostly shallow cleft with a size of ~20 × 10 × 7 $Å^3$ located between the dinucleotide binding and dimerization domains of each monomer (Fig. 2). The cleft extends toward the protein interior forming the active site region with the catalytic residues Cys^{153} and His^{248} (MCR of *S. todokaii* nomenclature) both strictly conserved in the GADPH-like family and reminiscent to thiol proteases (21). The molecular basis for substrate binding has been established by solving the structure of MCR_{NADP} at 1.9 Å resolution and of MCR_{CoA} at 2.4 Å resolution (Table 1). Comparisons between $MCR_{substrate\text{-}free}$, MCR_{NADP}, and MCR_{CoA} structures at the substrate binding cleft resulted in C_α deviations of maximally 0.9 Å. They are mostly below 0.3 Å.

$NADP^+$ Binding—The structure of MCR_{NADP} revealed a highly occupied $NADP^+$ molecule in an S-shaped conformation (Fig. 3*A*), which resembles that found in the ASD-$NADP^+$ and GAPDH-$NADP^+$-structures (22, 23). $NADP^+$ is positioned along the C-terminal side of the central β-sheet of the dinucleotide binding domain partly capped by the protruding cover loop that bridges strand 171:180 and 199:202 of the dimerization domain (Fig. 2). The 2′-phospho-ADP moiety is primarily attached to the dinucleotide recognition loop $^{14}GxxGxxG^{20}$. The 2′-phospho group of ribose is accommodated into a well designed pocket formed besides the dinucleotide recognition loop by the expanded hairpin-shaped segment linking strands 37:40 and 82:89. It is anchored to the polypeptide by multiple proton donors partly via a solvent molecule (Fig. 3*A*). This strong fixation of the phosphate group also provides the molecular basis for the specificity of NADPH against NADH and thus confirms the kinetic data (7). In comparison, the phospho group of the most related *M. jannaschii*

ASD is more exposed and the number of hydrogen bond contacts with the polypeptide significantly reduced compared with MCR. This difference rationalizes its dual specificity for NADPH and NADH as electron donor, albeit still with a clear preference for NADPH (18). As expected, the diphosphate group is sandwiched between the dinucleotide recognition loop and the conserved cover loop region ^{183}SGAGY^{187}; hydrogen bonds are formed between the α-phosphate oxygens and residues Leu^{18} NH and Tyr^{187} NH (Fig. 3*A*). A minor displacement of the cover loop upon $NADP^+$ binding shrinks the binding site of the phenol group of Tyr^{187}, which is rotated about 90° toward the bulk solvent. A crucial function in diphosphate binding is attributed to the second dimer of tetrameric MCR, as mutual interactions between the two cover loops (*i.e.* Arg^{153} and Asp^{194}) rigidify their conformations relative to each other (Fig. 2). A similar contact was found in GADPH (23).

The conformation of the catalytically competent ribose-nicotinamide moiety is related to that of other members of the GADPH family. Notably, Asn^{335}, Ser^{183} (part of the SG*x*G motif conserved in MCR and ASD), and the β-phosphate are hydrogen-bonded with the amide group of the nicotinamide group and fixes the latter in an optimal position for hydride transfer (Fig. 3*A*). The hydride transferring C4 atom of $NADP^+$ (and presumably of NADPH) and the thioacyl group of the Cys^{153} malonyl model (see below) are in van der Waals distance, which supports the functional relevance of the obtained nicotinamide conformation.

CoA Binding—Co-crystallization experiments between MCR and malonyl-CoA or succinyl-CoA resulted in a structure of MCR in complex with CoA (MCR_{CoA}), suggesting that its malonyl/succinyl head group was hydrolyzed during the crystallization process (Fig. 3*B*). The MCR_{CoA} structure revealed an identical binding site for CoA and $NADP^+$. Similar to $NADP^+$, CoA is present in an S-shaped, rather compressed conformation that is reflected in several intramolecular contacts (Fig. 3*B*).

When superimposing the MCR_{NADP} and MCR_{CoA} structures, $NADP^+$ and CoA globally align fairly well but not necessarily their analogous parts (Fig. 3*C*). Accordingly, the binding positions of the adenine rings are identical albeit mutually rotated and the 3′-ribose phosphate group of CoA approximately occupies the site of the 2′-ribose phosphate of $NADP^+$ (Fig. 3*B*). In addition, the diphosphate and the ribose of CoA are shifted ~2 Å away from the active site implicating that the β-phosphate of CoA occupies the site of the α-phosphate of $NADP^+$. The pantoate part of CoA approximately occupies the position of the β-phosphate of $NADP^+$, the β-alanine that of ribose, and the β-cysteamine that of the nicotinamide moiety (Fig. 3*C*).

CoA is primarily anchored to the polypeptide via its 3′-ribose phosphate using the same binding pocket as the 2′-ribose phosphate group of $NADP^+$ and its β-phosphate, which is strongly fixed between the dinucleotide binding and the cover loop (Fig. 3*B*). The latter anchor site is occupied by a phosphate (sulfate) in the $MCR_{substrate\text{-}free}$ structure documenting its high phosphate affinity. The residual components of CoA, also the α-phosphate, are essentially connected by unspecific van der Waals contacts. The more flexible pantetheine part is placed in an oversized binding site, and the number of contacts to the polypeptide is small (Fig. 3*B*). Solely, the terminal β-cysteamine sulfur forms polar interactions to Asn^{335} and Cys^{153}. The distance between the sulfurs (~3.1 Å) does not argue for a disulfide bond but rather for a hydrogen bond, similar to the interaction between the Cys^{153} thiolate and the (protonated) thiol group of CoA. However, in two subunits of the asymmetric unit, the β-cysteamine is largely disordered, and a highly flexible Cys^{153} adduct appears to be formed. We interpret the electron density as a mixture between Cys^{153} and CoA in a reduced and in an oxidized disulfide state. A covalent Cys^{153} CoA adduct has also been found in acetaldehyde dehydrogenase (24). We assume that the binding of malonyl/succinyl-CoA (not only CoA) with the strongly bound malonyl/succinyl (see below) rigidifies the β-cysteamine.

One Binding Site for Both $NADP^+$ and CoA—Enzymatic ping pong reactions are characterized either by covalent polypeptide (coenzyme)-ligand intermediates (25) or by prosthetic groups such as FAD that can store electrons (26). The consecutive binding of two substrates to the corresponding enzyme in principle allow them to share one binding site. Overlapping binding sites for NAD and CoA have been reported on the basis of hydrogen-deuterium exchange and mass spectrometric experiments for acetaldehyde dehydrogenase, another member of the GAPDH family (27, 28). The MCR_{NADP} and MCR_{CoA} structures, presented here, provide detailed insights into the architecture of a bispecific binding site that can host two large and structurally different cofactors. From the viewpoint of molecular engineering, this challenge might be responded by constructing an equivalent and high affinity binding site for the common ADP part of $NADP^+$ and CoA and flexible polypeptide segments that become selectively rearranged and fixed upon NADP and CoA binding, respectively. ADP as major component for $NADP^+$ binding has also been experimentally verified by ASD of *M. jannaschii* structurally related to MCR (18). Interestingly, nature adopts another strategy by essentially utilizing the protein as a rigid template that presses the conformationally variable coenzymes into highly similar S-shaped conformations (Fig. 3*C*). CoA and $NADP^+$ are surprisingly well superimposable, implicating that the β-phosphate of CoA is positioned on the α-phosphate in $NADP^+$ and the 3′- on the 2′-ribose phosphate of CoA and $NADP^+$, respectively. This shape/size-controlled cofactor binding forces the common ADP parts into different binding modes but smartly considers the increased length of pantetheine compared with the more voluminous ribose-nicotinamide part as well as the displacement of 3′- and 2′-ribose phosphate groups in CoA and $NADP^+$, respectively (Fig. 3*C*). In addition, the adjusted conformation allows both coenzymes to use the same tailor made ribose phosphate binding pocket as major fixation point (Fig. 3, *A* and *B*), which ensures, in parallel, the specificity for NADPH relative to NADH (7). Although remarkably superimposable, the slightly different surface profile of $NADP^+$ and CoA is accounted by tiny side chain rearrangements of contacting residues below 1.0 Å and by evading into the free space of the adjacent solvent.

The described template-governed cofactor shaping requires a strongly fixed and rigid substrate binding cleft that is presum-

ably provided by the compact globular domains and the multiple domain-domain and oligomeric interactions (Fig. 2). A crucial factor might also be the stabilization of the cover loop by tetramerization.

Evolution of the Bispecific Binding Site—MCR has evolved from ASD and, consequently, the bispecific binding site for $NADP^+$ and CoA originate from an $NADP^+$ binding site. The direction of evolution is weakly reflected on the atomic scale by the increased and more equally distributed enzyme-$NADP^+$ compared with the enzyme-CoA interactions and the unusually compressed conformation of CoA that is related to that of $NADP^+$ (Fig. 3*C*). CoA is normally found in a more elongated conformation even in those CoA-dependent enzymes that use, similar to MCR a dinucleotide binding domain for CoA binding (29, 30).

Comparison between ASD-$NADP^+$ and MCR-$NADP^+$ structures should provide information about how an $NADP^+$ is converted into an $NADP^+$ and CoA binding site. However, analysis is intricate, as the additional CoA specificity is accomplished by many amino acid exchanges at and far away from the cofactor binding site; three pronounced features are described in more detail. First, the shape/size of the ribose-phosphate binding pocket is modified by the conformationally changed hairpin segment between strands 37:40 and 82:89, in particular, due to the exchange of two residues in ASD by one residue (Gly^{42}) in MCR. This change provides space at the ribose phosphate binding site for the 3′-phosphate of CoA (Fig. 3*B*). For forming optimal polypeptide-phosphate interactions, the 2′-ribose phosphate of $NADP^+$ is moved toward 3′-ribose phosphate of CoA compared with that of the ASD-$NADP^+$ complexes. As a consequence, the adenine ring has to be rotated, which is compensated by the exchange of a small residue at position 41 in ASD by lysine in MCR and of a medium-sized residue such as leucine or threonine at position 91 by an alanine. This finding indicates an adaptation of the $NADP^+$ position to chemical restraints imposed by the CoA structure. Second, the interactions between the β-/α-phosphate of CoA/$NADP^+$ and Tyr^{187} implicates a small rearrangement of this region primarily caused by the mentioned altered hairpin segment and a hydrogen bond to Asp^{194} of the partner dimer (not present in dimeric ASD). Thus, tetramerization might also be used as a tool to optimize the common binding site for the β-/α-phosphate of CoA/$NADP^+$. Third, the ribose-nicotinamide binding site is geometrically conserved but appears to be more unpolar in MCR than in ASD reflecting the increased hydrophobicity of the pantetheine part of CoA. Thus, residues similar to alanine and serine in positions 18, 86, and 111 are replaced by a leucine and two prolines. In addition, the polar amide group of Asn^{94} is turned away in MCR but directed to the nicotinamide binding site in ASD. Asn^{94} becomes hydrogen bonded to Tyr^{23} in MCR that is substituted in ASD by an unpolar residue, mostly a methionine.

Substrate Binding and Catalyzed Reaction—A reaction cycle for the MCR reaction was already postulated (7), consisting of a nucleophilic attack of the Cys^{153}-thiolate onto the malonyl/succinyl-CoA thioester bond forming a covalent enzyme-malonyl/succinyl adduct. Its relatively stable thioacyl bond is subsequently reduced to malonic/succinic semialdehyde by

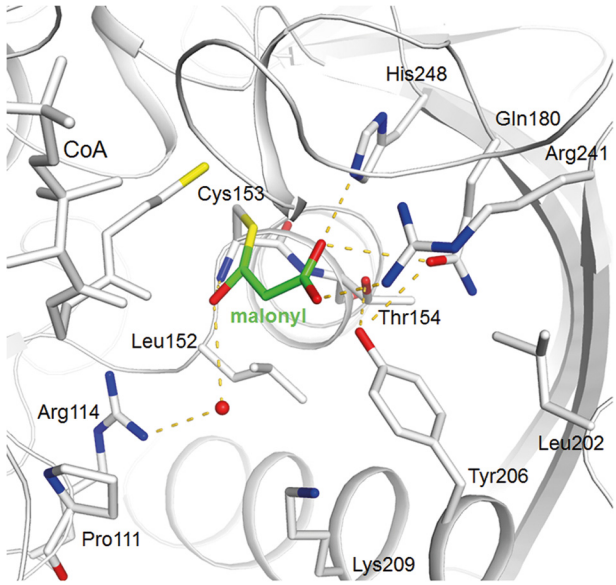

FIGURE 4. **Binding of the enzyme-malonyl thioacyl adduct.** The Cys^{153}-malonyl adduct (malonyl carbons in *green*) of MCR is modeled on the basis of the corresponding cysteine-aspartyl template of ASD. Although the thioacyl and the carboxylate surroundings of malonyl and aspartyl are highly conserved, the absence of the ammonium group tracks with an exchange of a glutamate and an asparagine in ASD with a tyrosine (Tyr^{206}) and a leucine (Leu^{152}) in MCR, respectively.

NADPH (Fig. 1). The presented structural data support this proposal and revealed a remarkable relationship between the active sites of MCR and ASD that allows a direct application of the wealth of structural and mechanistic data available for ASD (13). This high degree of conservation, despite substantial differences of the substrates used, becomes comprehensible when considering similarities between the aspartate and malonate/succinate and the CoA and $NADP^+$ structures as well as between the catalyzed reactions. In either case, an activated ester is reduced to an aldehyde with NADPH as electron donor (Fig. 1). Accordingly, the catalytic key players of MCR and ASD, the nucleophile Cys^{153}, the acid/base catalyst His^{248}, and most of the residues binding malonyl/succinyl or aspartyl, are found in similar positions. Therefore, a covalent MCR-malonyl/succinyl adduct can be transferred from the superimposed ASD-aspartyl template (31) without any interference with the surrounding protein matrix of MCR (Fig. 4). In addition, the distance of ca. 3.5 Å between the thioacyl carbon and the hydride donating C4 atom of the experimentally determined $NADP^+$ is reasonable for a hydride transfer and justifies the modeling operation. Consequently, the experimentally determined CoA and the deduced malonyl/succinyl binding positions (18) allow a reliable modeling of malonyl-CoA and, together with the found $NADP^+$ position, the postulation of a structure-based enzymatic mechanism for the MCR reaction (Fig. 5).

In complete agreement with the structure of the ASD-aspartyl thioacyl adduct (22, 31), the malonyl group is mainly anchored to the polypeptide via its carboxylate group by forming hydrogen bonds with the strictly conserved residues Gln^{180}, Arg^{241}, and His^{248} (Fig. 4). In addition, Arg^{241} appears to be the key amino acid to provide the promiscuity of MCR. The conformational variability of its side chain and of the loop following

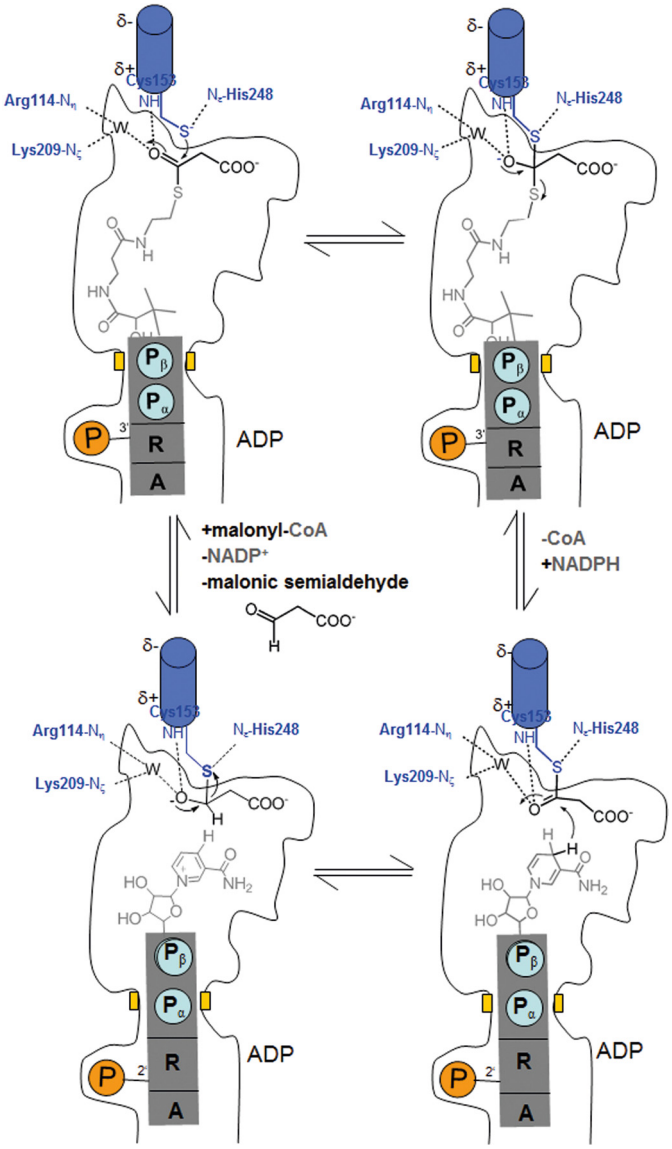

FIGURE 5. **Proposed enzymatic mechanism.** *A*, malonyl-CoA is bound and subsequently attacked by the Cys^{153} thiolate forming a tetrahedral intermediate. The negative charge of the oxyanion is stabilized by basic residues and by the positively charged N-terminal end of helix 152:168. *B*, the tetrahedral intermediate is converted to a thioacyl adduct, CoA is released, and NADPH is bound. CoA and NADPH use an identical binding site. *C*, NADPH transfers a hydride from the B-side to the thioacyl carbon forming a hemithioacetal intermediate, which is converted to the product malonic semialdehyde, thereby restoring Cys^{153} (*D*).

strand 233:241 (Fig. 4) allows accommodation of both malonyl- and succinyl-CoA that are distinguished by one methylene group (Fig. 1) (10).

The thioacyl oxygen of the modeled enzyme malonyl adduct most likely interacts with Arg^{114} $N_{\eta1}/N_{\eta2}$ and Lys^{209} N_{ζ} (after rigidification upon substrate binding) via a modeled water molecule and with Cys^{153} NH and/or Thr^{154} NH, both located at the positively charged N-terminal end of helix 152:168 (Fig. 4). This positively charged oxygen surrounding is well suited for stabilizing the tetrahedral oxoanion intermediate generated during catalysis (Fig. 5), either directly by charge compensation, or by activating the water molecule that may act as proton donor/acceptor. Oxoanion stabilization might also be the reason for the stimulation of the catalyzed reaction with Mg^{2+} ions (7).

Malonyl/succinyl is mainly distinguished from aspartyl by the absent positively charged ammonium group (Fig. 1), which interacts in ASD with invariant glutamate and asparagine side chains (18). In MCR, these residues are replaced by a tyrosine (Tyr^{206}) and a leucine (Leu^{152}); both strictly conserved residues contact the methylene group of malonyl/succinyl and are interpreted as the response of the more apolar character of malonyl/succinyl compared with aspartyl. Tyr^{206}, in contact to Leu^{152}, Thr^{154} (Ser in ASD), Gln^{180}, and Leu^{202}, maintains on one hand the hydrogen bond network important for malonyl carboxylate binding and catalysis and on the other hand maintains the position/conformation of Leu^{152} in a highly polar environment (Fig. 4). Its introduction required an unpredictable rearrangement of the N-terminal side of helix 203:220 compared with ASD (*i.e.* Ile → Gly^{203}, Lys → Asp^{204}). The resulting outward shift of Tyr^{206} prevents an interference of its long side chain with malonyl binding. In contrast, the stretch containing Leu^{152} is nearly identical in MCR and ASD reflecting its importance for catalysis (next residue, Cys^{153}). Leu^{152} would not only interfere with the ammonium group of aspartyl-4-phosphate but also with its phosphate group. A possible ASD activity is thus suppressed in agreement with kinetic data, indicating that $NADP^+$ is hardly reduced by malonic semialdehyde and phosphate (7).

Engineered Enzyme—A planned enzyme-based methacrylate synthesis pathway involves the reduction of 2-methylmalonyl-CoA to the corresponding semialdehyde, which requires the transformation of MCR to a productive methylmalonyl-CoA reductase. The structure of MCR is essential for substrate engineering as the exact surrounding of the new methyl group differs from that of ASD in an unpredictable manner. Broad mutational experiments are promising especially as attractive side chains exist and no significant large-scale conformational changes are expected upon substrate binding. The increased hydrophobicity around the methylene group of malonyl/succinyl in MCR compared with the ammonium group in ASD is, in principle, favorable; however, Leu^{152} would interfere with a methyl substituent, suggesting its exchange to a smaller residue such as valine, threonine, or alanine. Other side chains in the environment of the methyl group are Tyr^{206} (~3 Å), Lys^{209} (4 Å), and Pro^{111} (6 Å). Pro^{111} is especially interesting because of its more indirect participation in substrate binding and its position in a loop that might be variably designed.

Acknowledgments—We thank Hartmut Michel for continuous support and the staff of the beamline PXII at the Swiss Light Source (Villigen) for help during data collection.

REFERENCES

1. Burton, N. P., Williams, T. D., and Norris, P. R. (1999) Carboxylase genes of *Sulfolobus metallicus*. *Arch. Microbiol.* **172,** 349–353
2. Chuakrut, S., Arai, H., Ishii, M., and Igarashi, Y. (2003) Characterization of a bifunctional archaeal acyl coenzyme A carboxylase. *J. Bacteriol.* **185,** 938–947
3. Norris, P., Nixon, A. and Hart, A. (1989) Acidophilic, mineral-oxidizing bacteria: the utilization of carbon dioxide with particular reference to autotrophy in *Sulfolobus* in *Microbiology of Extreme Environments and Its*

Potential for Biotechnology (Da Costa, M. S., Duarte, J. C., and Williams, R. A. D., eds), pp. 24–39, Elsevier, London, United Kingdom) Elsevier, London, United Kingdom
4. Menendez, C., Bauer, Z., Huber, H., Gad'on, N., Stetter, K. O., and Fuchs, G. (1999) Presence of acetyl coenzyme A (CoA) carboxylase and propionyl-CoA carboxylase in autotrophic Crenarchaeota and indication for operation of a 3-hydroxypropionate cycle in autotrophic carbon fixation. *J. Bacteriol.* **181,** 1088–1098
5. Ishii, M., Miyake, T., Satoh, T., Sugiyama, H., Oshima, Y., Kodama, T., and Igarashi, Y. (1996) Autotrophic carbon dioxide fixation in *Acidianus brierleyi*. *Arch. Microbiol.* **166,** 368–371
6. Berg, I. A., Kockelkorn, D., Buckel, W., and Fuchs, G. (2007) A 3-hydroxypropionate/4-hydroxybutyrate autotrophic carbon dioxide assimilation pathway in Archaea. *Science* **318,** 1782–1786
7. Alber, B., Olinger, M., Rieder, A., Kockelkorn, D., Jobst, B., Hügler, M., and Fuchs, G. (2006) Malonyl-coenzyme A reductase in the modified 3-hydroxypropionate cycle for autotrophic carbon fixation in archaeal *Metallosphaera* and *Sulfolobus* spp. *J. Bacteriol.* **188,** 8551–8559
8. Hügler, M., Menendez, C., Schägger, H., and Fuchs, G. (2002) Malonyl-coenzyme A reductase from *Chloroflexus aurantiacus*, a key enzyme of the 3-hydroxypropionate cycle for autotrophic CO(2) fixation. *J. Bacteriol.* **184,** 2404–2410
9. Zarzycki, J., and Fuchs, G. (2011) Coassimilation of organic substrates via the autotrophic 3-hydroxypropionate bi-cycle in *Chloroflexus aurantiacus*. *Appl. Environ. Microbiol.* **77,** 6181–6188
10. Kockelkorn, D., and Fuchs, G. (2009) Malonic semialdehyde reductase, succinic semialdehyde reductase, and succinyl-coenzyme A reductase from *Metallosphaera sedula*: enzymes of the autotrophic 3-hydroxypropionate/4-hydroxybutyrate cycle in Sulfolobales. *J. Bacteriol.* **191,** 6352–6362
11. Evguenieva-Hackenberg, E., Schiltz, E., and Klug, G. (2002) Dehydrogenases from all three domains of life cleave RNA. *J. Biol. Chem.* **277,** 46145–46150
12. Cieśla, J. (2006) Metabolic enzymes that bind RNA: yet another level of cellular regulatory network? *Acta Biochim. Pol.* **53,** 11–32
13. Viola, R. E., Faehnle, C. R., Blanco, J., Moore, R. A., Xuying, L., Arachea, B. T., and Pavlovsky, A. G. (2011) The Catalytic Machinery of a Key Enzyme in Amino Acid Biosynthesis. *Amino Acids* **2011**
14. Suzuki, T., Iwasaki, T., Uzawa, T., Hara, K., Nemoto, N., Kon, T., Ueki, T., Yamagishi, A., and Oshima, T. (2002) *Sulfolobus tokodaii* sp. nov. (f. *Sulfolobus* sp. strain 7), a new member of the genus *Sulfolobus* isolated from Beppu Hot Springs, Japan. *Extremophiles* **6,** 39–44
15. Kawarabayasi, Y., Hino, Y., Horikawa, H., Jin-no, K., Takahashi, M., Sekine, M., Baba, S., Ankai, A., Kosugi, H., Hosoyama, A., Fukui, S., Nagai, Y., Nishijima, K., Otsuka, R., Nakazawa, H., Takamiya, M., Kato, Y., Yoshizawa, T., Tanaka, T., Kudoh, Y., Yamazaki, J., Kushida, N., Oguchi, A., Aoki, K., Masuda, S., Yanagii, M., Nishimura, M., Yamagishi, A., Oshima, T., and Kikuchi, H. (2001) Complete genome sequence of an aerobic thermoacidophilic crenarchaeon, *Sulfolobus tokodaii* strain7. *DNA Res.* **8,** 123–140
16. Kabsch, W. (1993) Automatic processing of rotation diffraction data from crystals of initially unknown symmetry and cell constants. *J. Appl. Cryst.* **26,** 795–800
17. Kissinger, C. R., Gehlhaar, D. K., and Fogel, D. B. (1999) Rapid automated molecular replacement by evolutionary search. *Acta Crystallogr. D Biol. Crystallogr.* **55,** 484–491
18. Faehnle, C. R., Ohren, J. F., and Viola, R. E. (2005) A new branch in the family: structure of aspartate-β-semialdehyde dehydrogenase from *Methanococcus jannaschii*. *J. Mol. Biol.* **353,** 1055–1068
19. Emsley, P., and Cowtan, K. (2004) Coot: model-building tools for molecular graphics. *Acta Crystallogr. D Biol. Crystallogr.* **60,** 2126–2132
20. Murshudov, G. N., Vagin, A. A., and Dodson, E. J. (1997) Refinement of macromolecular structures by the maximum-likelihood method. *Acta Crystallogr. D Biol. Crystallogr.* **53,** 240–255
21. Storer, A. C., and Ménard, R. (1994) Catalytic mechanism in papain family of cysteine peptidases. *Methods Enzymol.* **244,** 486–500
22. Faehnle, C. R., Le Coq, J., Liu, X., and Viola, R. E. (2006) Examination of key intermediates in the catalytic cycle of aspartate-β-semialdehyde dehydrogenase from a gram-positive infectious bacteria. *J. Biol. Chem.* **281,** 31031–31040
23. Skarzyński, T., Moody, P. C., and Wonacott, A. J. (1987) Structure of holo-glyceraldehyde-3-phosphate dehydrogenase from *Bacillus stearothermophilus* at 1.8 A resolution. *J. Mol. Biol.* **193,** 171–187
24. Smith, L. T., and Kaplan, N. O. (1980) Purification, properties, and kinetic mechanism of coenzyme A-linked aldehyde dehydrogenase from *Clostridium kluyveri*. *Arch. Biochem. Biophys.* **203,** 663–675
25. Ferrer, J. L., Jez, J. M., Bowman, M. E., Dixon, R. A., and Noel, J. P. (1999) Structure of chalcone synthase and the molecular basis of plant polyketide biosynthesis. *Nat. Struct. Biol.* **6,** 775–784
26. Pejchal, R., Sargeant, R., and Ludwig, M. L. (2005) Structures of NADH and CH3-H4folate complexes of *Escherichia coli* methylenetetrahydrofolate reductase reveal a spartan strategy for a ping-pong reaction. *Biochemistry* **44,** 11447–11457
27. Lei, Y., Pawelek, P. D., and Powlowski, J. (2008) A shared binding site for NAD+ and coenzyme A in an acetaldehyde dehydrogenase involved in bacterial degradation of aromatic compounds. *Biochemistry* **47,** 6870–6882
28. Manjasetty, B. A., Powlowski, J., and Vrielink, A. (2003) Crystal structure of a bifunctional aldolase-dehydrogenase: sequestering a reactive and volatile intermediate. *Proc. Natl. Acad. Sci. U.S.A.* **100,** 6992–6997
29. Wolodko, W. T., Fraser, M. E., James, M. N., and Bridger, W. A. (1994) The crystal structure of succinyl-CoA synthetase from *Escherichia coli* at 2.5-A resolution. *J. Biol. Chem.* **269,** 10883–10890
30. Ricagno, S., Jonsson, S., Richards, N., and Lindqvist, Y. (2003) Formyl-CoA transferase encloses the CoA binding site at the interface of an interlocked dimer. *EMBO J.* **22,** 3210–3219
31. Blanco, J., Moore, R. A., and Viola, R. E. (2003) Capture of an intermediate in the catalytic cycle of L-aspartate-β-semialdehyde dehydrogenase. *Proc. Natl. Acad. Sci. U.S.A.* **100,** 12613–12617